



# Impact of hydration stoppage on quantification of the GGBS content in ternary limestone cements using the PONKCS method

Samuel Adu-Amankwah · Maciej Zajac · Pengkun Hou · Leon Black

Received: 13 June 2022 / Accepted: 16 April 2023 / Published online: 12 July 2023  
© The Author(s) 2023

**Abstract** Most supplementary cementitious materials (SCMs) are predominantly poorly-crystalline or amorphous. Their reactivity is routinely evaluated through SEM image analysis (SEM/IA), which is a laborious and resource intensive technique. Quantitative X-ray diffraction (QXRD) provides an alternative, facilitating simultaneous evaluation of reaction kinetics and phase assemblages. However, QXRD requires relevant model structures, which are lacking for amorphous phases. In this study, we use the Phases of No Known Crystal Structures (PONKCS) method to model and calibrate ground granulated blast furnace slag (GGBS) and assess robustness in quantifying the

GGBS content in synthetic and hydrated ternary blended CEM I-GGBS-limestone cements. Implications of sample preparation, in particular hydration stopping methods on the quantification was measured via the external standard method. Subsequently, the results are compared with SEM/IA calculations, based on backscattered images and magnesium maps. Robustness of the calibrated PONKCS phase is demonstrated with and without hydration stopping. However, X-ray absorption by the cements must be accounted in the attenuation co-efficient calculation. Freeze-drying destroyed water-rich phase assemblages and led to overestimation of the calibrated GGBS phase contents.

**Supplementary Information** The online version contains supplementary material available at <https://doi.org/10.1617/s11527-023-02198-6>.

S. Adu-Amankwah (✉)  
Department of Civil Engineering, Aston University, Aston St, Birmingham B4 7ET, UK  
e-mail: s.adu-amankwah@aston.ac.uk

S. Adu-Amankwah · L. Black  
School of Civil Engineering, University of Leeds, Woodhouse Ln., Leeds LS2 9JT, UK

M. Zajac  
Global R&D HeidelbergCement AG, Oberklamweg 2-4, 69181 Leimen, Germany

P. Hou  
Department of Materials Science and Engineering, University of Jinan, Jinan, Shandong, China

**Keywords** Ternary limestone cement · PONKCS/QXRD · Hydration stopping · Phase assemblages

## 1 Introduction

Quantitative evaluation of the reaction kinetics and products of hydration in blended cements is an important step towards production of low carbon cement concrete. Numerous techniques e.g. selective dissolution, scanning electron microscopy, calorimetry, thermogravimetric analysis, and mass balance calculations have been employed to study these [1–5]. Ternary limestone-GGBS cements are of interest in



this contribution due to their growing popularity and susceptibility of their water-rich phase assemblages to various hydration-stopping approaches.

In most hydration and microstructure investigations, free water in the cement has to be removed to enable age-dependent studies. Some techniques including porosimetry and SEM require sample drying in order to characterize the pore structures. To this end, different hydration stopping regimes have been reported and reviewed in the literature [6, 7]. These techniques simultaneously impact on the pore structure and the hydrated assemblages [8, 9] with the appropriateness of a method dependent on the objective of the microstructural investigation. Interactions between portlandite and organic solvents have been reported [10, 11]. Galan et al. [12] noted slight modifications in the ettringite contents after solvent exchange while oven drying destroyed ettringite. Snoeck et al. [13] examined the implications of hydration stopping techniques on bound water and the calcium silicate hydrate (C-S-H) content. The portlandite (CH) content was not significantly altered in any of the investigated methods other than freeze-drying and oven drying. Solvent exchange as well as vacuum drying were found to be least detrimental to the C-S-H and the chemically bound water. With respect to portlandite preservation, similar conclusions were made in the RILEM round robin test [14], but lower ettringite and carboaluminate contents were calculated after hydration stopping. For the solvent exchange or vacuum drying methods, varied protocols and duration in the solution or under vacuum are reported in the literature [5–7, 13]. For example, Kakali et al. [15] implemented a 24 h vacuum drying and successfully identified poorly crystalline AFm assemblages in limestone containing cements. Snellings et al. [16] removed free water by storing samples in iso-propanol for 7 days followed by storage in a desiccator. Meanwhile, double solvent exchange involving iso-propanol and diethyl, or petroleum ether have been used extensively [17–20] and reported to preserve most phase assemblages. The implications of different hydration stopping methods on quantitative phase analysis of hydrated cement has received only limited consideration [6, 12, 14].

Many authors have successfully used Scanning Electron Microscopy image analysis (SEM/IA) to quantify the contents of cementitious materials [1, 4, 21–25], with  $\sim 5\%$  precision reported for the

technique [5]. The technique utilizes backscattered electron images of flatly-polished specimens, with compositions differentiated based on their grey-level histogram, which in turn depends on the mean local atomic number. The technique however, has drawbacks. For example, the large interaction volumes of backscattered electrons diminish the spatial resolution of images, causing underestimation of residual finer phases, whilst approximation of 3D features from 2D images induces stereological errors that are infrequently corrected in the cement literature. Besides, most SCMs have similar brightness to the hydrated phase assemblages in cements especially CH, causing overlap of the grey levels. Consequently, good quality elemental maps are required for segmentation [1, 4, 22]. This, when coupled with acquiring representative number of fields, which may take 5–10 h per specimen [1, 22], makes the technique laborious and resource intensive.

X-ray diffraction is one of the most versatile techniques for simultaneously monitoring reaction kinetics and phase assemblages. Compared to thermal analysis and SEM/IA, individual crystalline phases in the constituent materials can be analysed in addition to hydrated assemblages by matching the model structures of all known components to the observed diffraction trace while minimizing the error of the fit [26, 27]. Recently, QXRD analysis has been extended to evaluate the weight fractions of amorphous materials and phases that have partial or no known crystal structures (PONKCS) [16, 28–32]. The approach involves modelling the unknown or amorphous phase(s) and calibrating the model for subsequent implementation in the Rietveld refinement. The weight fractions of all phases whose crystal structures are included in the refinement including the calibrated amorphous phase can then be calculated by the internal standard [33], direct implementation of the ZMV algorithm [28, 34] or the external standard [35, 36] methods. The latter however requires consideration of the samples' X-ray absorptive characteristics. Superposition of the products of linear absorption [37] and weight fraction of the oxides present in the material is one approach for estimating this [36]. In hydrated cement, water (free and bound) can make up to 60% of the matrix depending on w/b ratio and age, which can modify the absorptive characteristics. More importantly, methods for removing free water can damage the microstructure and ultimately crystallinity



of some phases. These can present profound challenges when implementing the PONKCS phase for cements containing GGBS, since the slag exhibits overlapping halos with the C-S-H in hydrated cement and many of the water-rich hydrated phase assemblages are sensitive to hydration stoppage. The objective of this paper therefore is to elucidate impact of hydration stopping regimes on robustness of the calibrated PONKCS phase in hydrated ternary limestone-GGBS cement.

## 2 Materials and methods

### 2.1 Materials

The investigated samples were prepared from commercial grade CEM I 52.5 R, GGBS and limestone. These were used to prepare ternary cement at 5:4:1 ratio, with the sulphate content adjusted to 3%. For calibrating and testing the PONKCS phase for GGBS, synthetic mixes of GGBS and 99.99% purity corundum (supplied by Sigma Aldrich) were prepared. Composition of the constituents from XRF and mineralogy from XRD are shown in Tables 1 and 2 respectively. 100 g of the weighted components were homogenized in a roller ball mill at 300 revolutions/minute for 3 h using polymer balls to avoid further grinding.

**Table 1** XRF composition of materials

Material	CEM I	GGBS	Limestone	Corundum	
SiO <sub>2</sub>	20.37	34.87	2	–	
Al <sub>2</sub> O <sub>3</sub>	5.56	11.62	0.8	99.99	
TiO <sub>2</sub>	0.29	1.11	0.04	–	
MnO	0.05	0.27	0.03	–	
Fe <sub>2</sub> O <sub>3</sub>	2.49	0.45	0.32	–	
CaO	62.1	41.82	53.13	–	
MgO	1.65	5.82	0.64	–	
K <sub>2</sub> O	0.65	0.47	0.1	–	
Na <sub>2</sub> O	0.07	0.07	–	–	
SO <sub>3</sub>	3.54	3.13	0.07	–	
P <sub>2</sub> O <sub>5</sub>	0.14	0.02	0.04	–	
LOI	1.99	(+ 1.45)	42.3	–	
Blaine Fineness, m <sup>2</sup> /kg	593	454	328	–	
The Brindley fineness parameter of GGBS 2 is given in bracket	MAC (μ), cm <sup>2</sup> /g	96.46	74.59	69.82	31.69
	Brindley coarseness (μD <sub>50</sub> ), cm <sup>3</sup> /g	0.095	0.059 (0.037)	0.014	0.006

Based on the mean particle size and sample's linear X-ray absorption, corundum is classified as having medium fineness while the cementitious materials have coarse fineness.

The particle size distribution of the materials as measured by laser granulometry with iso-propanol as dispersant are shown in Fig. 1.

### 2.2 Sample preparation

Two sets of samples were examined in this study— anhydrous/synthetic mixes and hydrated cement mixes. The anhydrous/synthetic mixes were:

- Synthetic blends of GGBS and corundum, prepared at 10:90, 15:85, 30:70 or 50:50 ratios
- Anhydrous blended cements prepared at 50:50 CEM I: SCM ratio, where 10 or 20% of the SCM was limestone and the remainder GGBS. In these cements, the sulphate content was maintained at 3% and the effect of GGBS fineness was also examined.

The hydrated cement pastes prepared from the ternary limestone blend comprising 50% CEM I, 40% GGBS and 10% limestone. The paste samples were prepared in accordance with EN 196-1 but without the aggregates (0.5 w/c ratio). These were cast into 10 mm diameter plastic vials and stored in a water bath maintained at 23 °C. Samples were analysed after 1, 2,

**Table 2** Mineralogical composition of CEM I and supplementary cementitious materials (%weight)

Phase	C <sub>3</sub> S	β-C <sub>2</sub> S	C <sub>3</sub> A	C <sub>4</sub> AF	Calcite	Anhydrite	Hemihydrate	Others*	ACn**
CEM I	58.1	14.3	9.2	6.7	1.9	1.7	3.0	1.3	3.8
GGBS					2.4			0.1	97.5
Limestone					96.6			1.4	2.0
Anhydrite						98.8		1.2	

\*Includes where applicable arcanite, dolomite, periclase and quartz

\*\*ACn comprises amorphous, misfit and non-determined contents

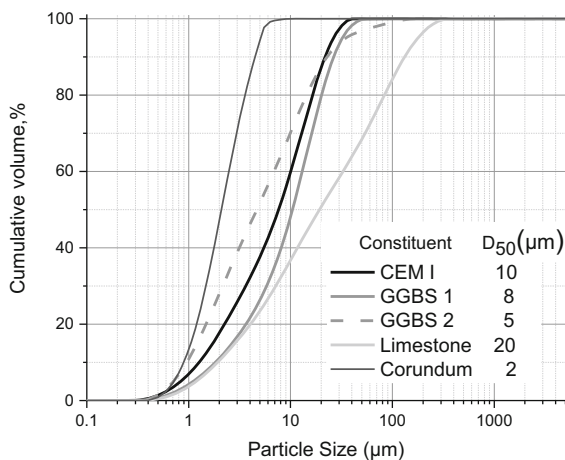


**Fig. 1** Particle size distribution of constituent materials, determined by laser granulometry. Note: The effect of fineness of the amorphous phase was studied by grinding the same batch of GGBS in a ball mill. This finer material is referred to as GGBS 2

7 and 28 days of hydration. At the given age, XRD and TGA measurements were performed on freshly ground specimens (herein referred to fresh) or hydration stopped by one of three commonly employed methods, namely freeze drying (FD), combined solvent exchange and vacuum drying (SV), and double solvent exchange (DS). After each method, samples were stored in mini-grip bags in a glovebox until testing. The methods are subsequently described below:

### 2.2.1 Freshly ground samples (Fresh)

The rationale here was to preserve the hydrated assemblages and to retain water in the samples. Using a mortar and pestle, pastes were crushed and finely ground to pass a 63-micron sieve. Grinding and

packing of the powders into mini-grip bags were performed inside a nitrogen-purged glovebox. Subsequently, samples were analysed by XRD and TGA. The time between sample grinding and characterisation was approximately 10-min. Potential drying of the samples during grinding was assumed to be negligible whilst drying of the cements during the measurement was prevented by covering the samples with kapton tape [29, 32].

### 2.2.2 Freeze-drying (FD)

Freeze-drying aims to remove free water from the hydrating cement by sublimation. The 2 mm thick slices were cut from the hydrated cement cylinders using a low speed saw (Buehler Isomet) in a glovebox. These were weighed and immediately placed in liquid nitrogen where the pore water was frozen at  $\sim -196$  °C until the sample equilibrated with the liquid. Following, the slices were transferred to an Edwards Modulyo freeze drying chamber, maintained at  $-45 \pm 5$  °C under  $\sim 4.6$ -mm Hg atmosphere. The chamber was connected to an external vacuum pump, which removed the sublimate. The slices were weighed frequently until constant weight.

### 2.2.3 Solvent exchange followed by vacuum drying (SV)

Solvent exchange treatment dilutes capillary pore water with organic solvents which are in turn removed from the sample by drying. The characteristics of a range of solvents have been described elsewhere [7]. Suitability of iso-propanol (IPA) for cement hydration stopping is well documented in the literature [7, 38, 39]. IPA has greater diffusivity in water and has lower surface tension and vapour pressure



compared to other commonly used organic solvents and hence tends to be less aggressive to cement hydrates and the pore structure.

Here, 2 mm thick slices were cut from the hydrated cements using low speed isoment. These were immersed in IPA at a solid to liquid ratio of 1:500 by volume for 48-h. The samples were then transferred into a desiccator which was connected to a vacuum pump for 24 h to remove the solvent.

#### 2.2.4 Double solvent exchange using iso-propanol and diethyl ether (DS)

The rationale here was to reduce the cement exposure time to the organic solvent, which is good for studying short-term hydration, minimizing possible interaction with the hydrates and to ensure thorough removal of the IPA [18–20]. Freshly cut hydrated cement samples were crushed to  $\sim 1$  mm in IPA for 20 min inside a nitrogen-purged CO<sub>2</sub>-free glovebox. Maintaining the sample in the glovebox, the solvent was filtered under gravity and the residue rinsed with diethyl-ether for 10 min before drying at 40 °C on a preheated glass plate for a further 20 min.

### 2.3 Analytical methods

All fresh and hydration stopped samples were analysed by both TGA and XRD but SEM was performed only on freeze-dried samples.

TGA was performed on a Stanton Redcroft 780 Series Analyzer under nitrogen, purged at 58 ml/min. About 16–18 mg of ground sample was heated in a platinum crucible at a rate of 20 °C/min up to 1000 °C. The total water in the sample and CH contents were computed between 20–550 °C and  $\sim 400$ –500 °C from the TGA data using Eqs. (1–3) respectively. The contents were then normalized to the ignited weight at 550 °C to rescale the measured content per 100 g of anhydrous cement. This does not consider potential carbonation of portlandite during sample preparation, but such effects would be small in the samples in which hydration was arrested. The calcium carbonate content was also calculated from the TGA curve using Eq. (3) and the results similarly normalized to the ignited weight at 1000 °C.

$$W_t(\%) = \frac{(M_{20\text{ }^\circ\text{C}} - M_{550\text{ }^\circ\text{C}})}{M_{550\text{ }^\circ\text{C}}} * 100\% \quad (1)$$

$$\text{CH}(\%) = \frac{\text{CH}_{TG}74/18}{M_{550\text{ }^\circ\text{C}}} * 100\% \quad (2)$$

$$\text{C}_c(\%) = \frac{\text{C}_{cTG}100/44}{M_{1000\text{ }^\circ\text{C}}} * 100\% \quad (3)$$

where,  $W_t$  is the total water in the sample, CH is the measured portlandite content per 100 g of the anhydrous;  $\text{CH}_{TG}$  is % weight loss from water associated with calcium hydroxide,  $C_c$  is measured calcium carbonate content per 100 g of the anhydrous and  $\text{C}_{cTG}$  is the weight loss associated with carbon dioxide.  $M_{20\text{ }^\circ\text{C}}$  is the ignited weight at 20 °C;  $M_{550\text{ }^\circ\text{C}}$  is the ignited weight at 550 °C and  $M_{1000\text{ }^\circ\text{C}}$  is the ignited weight at 1000 °C. Note that  $\text{CH}_{TG}$  and  $\text{C}_{cTG}$  were calculated by the tangent method.

X-ray diffraction scans were obtained initially from synthetic mixes of GGBS with corundum and then with synthetic C-S-H of 1.33 and 1.5 Ca/Si ratio. Details of the C-S-H synthesis is reported elsewhere [40]. Anhydrous blended cements containing GGBS, CEM I and limestone were also scanned to evaluate the modelled GGBS phase. Subsequently, the hydrated cement pastes were scanned after stopping the hydration reaction by the above-described methods.

The finely ground powder samples were back-loaded into a 10 mm diameter metallic sample holder to minimize preferred orientation [41]. The data were acquired on a Phillips X'pert PANalytical MPD Pro, a Bragg–Brentano diffractometer, using a CuK $\alpha$  anode. The instrument was operated at 40 kV and 40 mA equipped with an X'Celerator detector, over a range of 5–80 ( $2\theta^\circ$ ) using a step size of 0.0334°. The continuous scan mode was adopted for all data recording and the data analysis was performed on TOPAS Academic software v4.2.

#### 2.4 Modelling and calibration of the PONKCS Phase for GGBS

The diffuse halo due to GGBS was modelled using a scan from pure GGBS using the fundamental parameter approach. The latter defines and fixes the instrument contributions to the peaks [42]. The instrument parameters were 240 mm goniometer radii and active



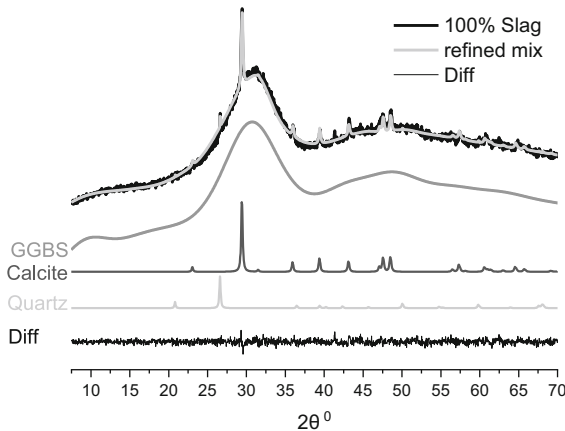


**Fig. 2** The Modelled GGBS phase for PONKCS calibration and deconvoluted calcite and quartz peaks

detector length of 2.122 ( $2\theta^\circ$ ). The incident x-ray beam had a fixed anti-scatter Soller slit with a beam mask of 10 mm and a programmable divergence slit, giving a constant irradiated length of 10 mm and a receiving Soller slit of  $2.3^\circ$ . These were defined and fixed for the modelling and calibration of the amorphous phase and in subsequent refinements.

A first order Chebyshev polynomial was used to describe the background. Fundamental parameter peak phase comprising 7 peaks were used to model the GGBS pattern while the small levels of calcite and quartz were refined using the structures of Maslen et al. [43] and Le Page [44] respectively. The number of peaks was chosen so that the model accurately described the specimen's diffraction pattern. The peaks were indexed and the best fit space group (in this case Ia-3d cubic) refined as an  $hkl$  phase using the Pawley method [45]. Deconvolution of the peaks and the resultant GGBS model together with the difference plot and the crystalline phases are illustrated in Fig. 2.

The refined lattice parameter  $a = b = c = 15.63 \text{ \AA}$ , crystallite size and volume for the modelled GGBS phase were then fixed for the calibration step. Calibration was performed on a 50% binary mixture with corundum. Here, only the scale factor was refined. The arbitrary ZM constant [28] was determined by re-arranging the internal standard Eq. (4) and the unit volume.

$$(ZM)_a = \frac{W_a \cdot S_{st}}{W_{st} \cdot S_a \cdot V_a} (ZMV)_{st} \quad (4)$$

where  $Z$  is the number of formula units per unit cell,  $M$  and is mass of unit cell,  $V$  is unit cell volume,  $S$  is scale factor of a phase,  $W$  is known weight in %,  $st$  denotes the reference standard, and  $a$  denotes the GGBS phase under calibration.

The structure files implemented in the Rietveld refinement (for the cement samples) were taken from the ICSD database. In generating the control file, the lattice parameters were initially refined on phase-enriched mixes after selectively dissolving interstitials in aqueous potassium hydroxide and sucrose solution, with the silicates being dissolved in a salicylic acid and methanol solution, following the procedures of Gutteridge [46]. The refined model phases were subsequently constrained and refined in the as received CEM I according to the recommendations of Le Saoût et al. [41].

The phase contents following the Rietveld refinements were obtained by the external standard method [35, 36] according to Eqs. (5 and 6). The reference standard, corundum (c), was scanned once per each data collection date, accounting for measurement-specific G-factor [35]. The latter accounted for potential ageing of the X-ray tube over time. The sample mass absorption co-efficient arising from the different techniques for arresting hydration in the cements were determined from the XRF data and the sample-specific total water contents and in the hydration stopped samples, the bound water contents using Eq. (7) according [47].

$$G = S_c \frac{\rho_c v_c^2 \mu_c}{C_c} \quad (5)$$

$$W_a = S_j \frac{\rho_a v_a^2 \mu_{\text{sample}}}{G} \quad (6)$$

$$\mu_{\text{sample}} = \sum w_i \mu_i \quad (7)$$

where  $\rho$  is phase density from unit cell volume and cell mass,  $\mu$  is the micro-absorption coefficients (MAC) of sample determined from Eq. (7),  $v$  is unit cell volume,  $G$  is calibration factor,  $C$  is the known crystalline content of reference standard and  $w_i$  is the % abundance of a component from XRF and in the hydrated systems include total water from TGA.

In order to scale-up the unreacted GGBS content in the hydrated samples to the anhydrous, the weight

fractions obtained from Eq. (6) were further normalized ( $W_\infty$ ) using Eq. (8) to account for dilution.

$$W_\infty = W_a \left[ 1 + \frac{W_t}{100} \right] \quad (8)$$

where  $W_t$  is the total water content from TGA as in Eq. (1).

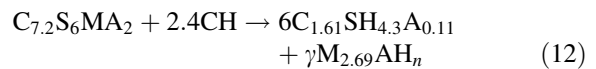
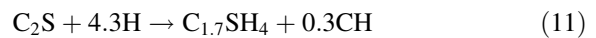
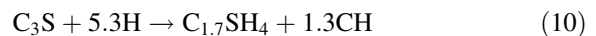
Samples for SEM were 2 mm thick freeze-dried slices. These were resin impregnated and polished down to 0.25  $\mu\text{m}$  using a combination of diamond paste and silicon carbide cloths. Images were acquired in backscattered electron mode using a Zeiss EVO MA15. The instrument was operated at 15 keV accelerating voltage with an 8.5 mm working distance. For each specimen 50 image fields were collected at  $800 \times$  magnification at  $1024 \times 768$  resolution giving the smallest observable features to be  $\sim 0.17 \times 0.17 \mu\text{m}$ . The corresponding magnesium maps were recorded with an 80 mm aperture EDS detector at 100,000 counts per second over a map acquisition time of 5 min per field.

The images were analysed using the open-source ImageJ programme according to the protocol illustrated in Fig. 3. The BSE images were automatically corrected for brightness and contrast and the thresholding performed using the grey level histogram shown in Fig. 3c. The minimum points bounding the grey level peaks were chosen to select the GGBS grains. Intermixing between GGBS and other phases especially CH was inevitable (Fig. 3c). Consequently, the thresholded region for GGBS with inclusions was initially binarized and inverted such that the region of interest was white with all other features assigned black. Subsequently, these were overlaid with magnesium maps prepared by increasing the contrast between the Mg containing regions and those without. Opacity for the overlay was set to 30% allowing the thresholded regions containing Mg to be segmented (Fig. 3e and f). The overlaid image was filtered (using the in-built smoothing function) to reduce noise and the area fraction of the segmented region (equivalent to the volume fraction) calculated as the unreacted GGBS content at the age of the specimen. The degree of hydration of GGBS was thus calculated from Eq. (9).

$$\text{DoH}_{\text{GGBS}} = \frac{(S_0 - S_t)}{S_0} \times 100\% \quad (9)$$

where,  $S_0$  is the initial volume of GGBS in the mix and  $S_t$  is the residual volume of GGBS after time,  $t$ .

In the hydrated systems, the expected quantities of C-A-S-H were determined from mass balance calculations based on the following reaction Eqs. (10–11). The composition of the as-received materials were based on XRF (GGBS) and clinker from (QXRD) data in Tables 1 and 2 while composition of the C-A-S-H phase was from SEM/EDX analysis [19]. The information about kinetics were based on the degrees of hydration of all components based on the quantitative phase analysis. This approach for determining the C-A-S-H content has been reported elsewhere [48].



### 3 Results and discussion

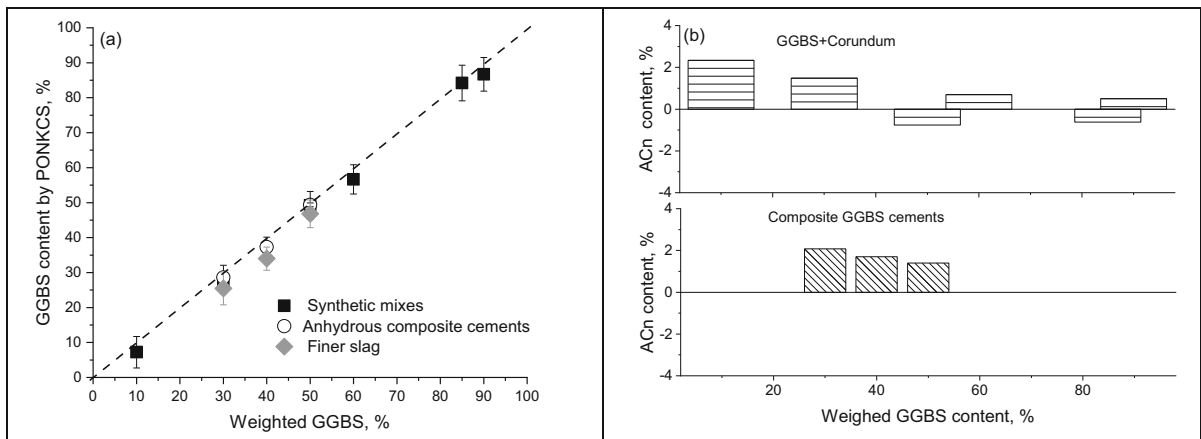
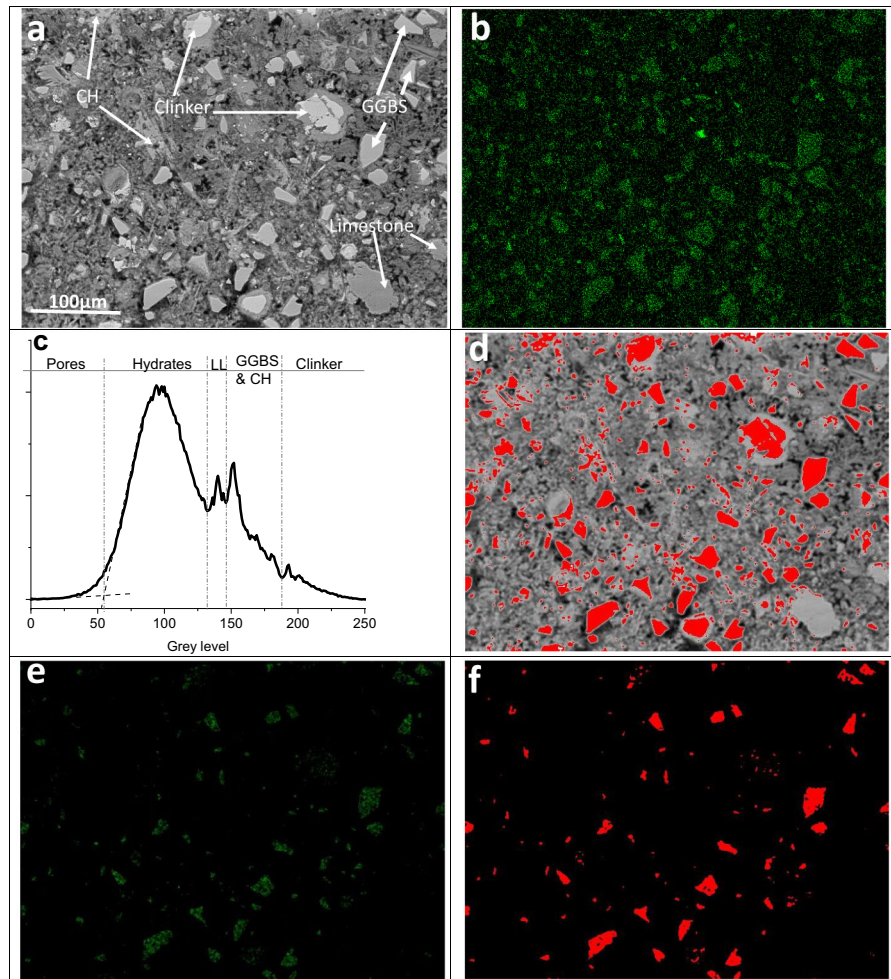
#### 3.1 Determination of the amorphous content by XRD

Figure 4a compares the weighted GGBS contents and those measured from the Rietveld refinement of the PONKCS phase in synthetic mixes with corundum, anhydrous binary and ternary cements of varying mix compositions and fineness. Quantification of the GGBS content is reasonable. Increased GGBS fineness (see Fig. 1) resulted in slight reduction in the measured amount, but well within the measurement error, possibly due to the narrow mean particle size range, 5–10  $\mu\text{m}$ , as opposed to those reported elsewhere [49]. The MAC of the binary mixtures with corundum, based on the XRF compositions ranged between 33 and 67  $\text{cm}^2/\text{g}$  while that in the blended cements were approximately 84  $\text{cm}^2/\text{g}$ .

The standard deviation of the quantification from three independent XRD scans were generally greater in the synthetic mixes than in the blended cements. For a given mix, the ZMV/K is constant [28, 50] and hence deviations may be ascribed to heterogeneous dispersion of corundum in GGBS (causing scale factor errors) and X-ray absorption during the measurement.



**Fig. 3** Protocol for extracting the residual GGBS content via Image J: **a** is Backscattered electron image; **b** is magnesium map **c** grey-level histogram; **d** thresholding to extract phase of interest showing overlapped phases based on grey levels; **e** overlaid magnesium map at 30% opacity and **f** segmented GGBS



**Fig. 4** **a** A plot of weighted GGBS content versus that measured by PONKCS and **b** A comparison of the non-determined phase (ACn) contents in the investigated mixes as a function of GGBS dosage

**Table 3** Effect of particle size on micro-absorption contrast in the investigated anhydrous mixes

Mix ID	Sample type	Corundum content (%)	GGBS content (%)	Mixture MAC ( $\mu$ )	Brindley correction (K)
S <sub>1</sub> -10C	Synthetic GGBS—corundum mixes	10	90	69.88	1.00
S <sub>1</sub> -30C		30	70	61.40	0.99
S <sub>1</sub> -50C		50	50	52.91	0.98
S <sub>1</sub> -60C		60	40	48.66	0.98
S <sub>1</sub> -85C		85	15	38.06	0.97
S <sub>1</sub> -90C		90	10	35.93	0.96
CS <sub>1</sub> 30-L	Anhydrous GGBS1 mixes		30	83.21	1.03
CS <sub>1</sub> 40-L			40	83.83	1.03
CS <sub>1</sub> 50-L			50	84.44	1.04
CS <sub>2</sub> 30-L	Anhydrous GGBS2 mixes		30	83.21	1.03
CS <sub>2</sub> 40-L			40	83.83	1.03
CS <sub>2</sub> 50-L			50	84.44	1.03

$K = 1 - \sum(\mu_i - \mu)D_i$ , after [51], where  $\mu_i$  and  $\mu$  are constituent and mixture MAC and  $D_i$  is constituent mean particle size

The latter could be induced differences in particle sizes of the constituents in the mixture, causing disproportionate absorptions and subsequent reductions in the X-ray intensities. Implementation of the Brindley correction (K) for multi-constituent mixtures has been suggested elsewhere [50, 51]. The parameter considers individual constituent absorptions and mean sample absorption, together with constituent particle sizes [51]. As shown in Table 3, the Brindley correction varies with the GGBS content. In the synthetic GGBS—corundum mixes, K decreased as the corundum content was raised but increasing trends, albeit small were seen in anhydrous blended cements. This means absorption induced errors in the quantification would be amplified in the synthetic mixes. For example, in the mixture containing 90% corundum, the GGBS phase reflection would be up to 4% lower relative to corundum due to the contrast in X-ray absorption and particle fineness (see Tables 1 and 3).

The non-determined contents (ACn), calculated indirectly by subtracting the total quantified phases (i.e. crystalline and PONKCS phase) from 100%, shown in Fig. 4b, was larger at low GGBS content. The X-ray micro-absorption contrast yet again offers a plausible explanation for this. Though the absorption contrast is small at higher corundum dosage (and low GGBS content), the GGBS is coarser and has a higher MAC (see Table 3), hence it absorbs more X-rays. This enhances the corundum peak intensities relative

to the background and plausibly reduces the amorphous phase quantified by the PONKCS method. Meanwhile, at similar GGBS levels, the ACn was slightly greater in the anhydrous blended cements compared to the synthetic mix due to the non-determined (ACn) content in the anhydrous CEM I as shown in Table 2. The foregoing highlight some of the challenges associated with the internal standard method of calibrating the PONKCS phase. However, implementation of the external standard methodology should address or minimize the micro-absorption induced errors.

### 3.2 Quantification of residual GGBS content in hydrated blended cements – pitfalls

#### 3.2.1 The C-A-S-H

In blended cements, latently hydraulic GGBS reacts in the presence of portlandite forming aluminium incorporated calcium silicate hydrate and hydrotalcite. These and reduced hump associated with GGBS are noticeable in the 20–40° 2 $\theta$  range, (Fig. 5a). The presence of water in the sample increases the background due to low scattering contributions. Although, water absorbs little radiation compared to the hydrates and unreacted cement, it comprises 33% of the volume in the non-hydration stopped samples. Micro-absorption is higher in the solid cement particles (Table 3)



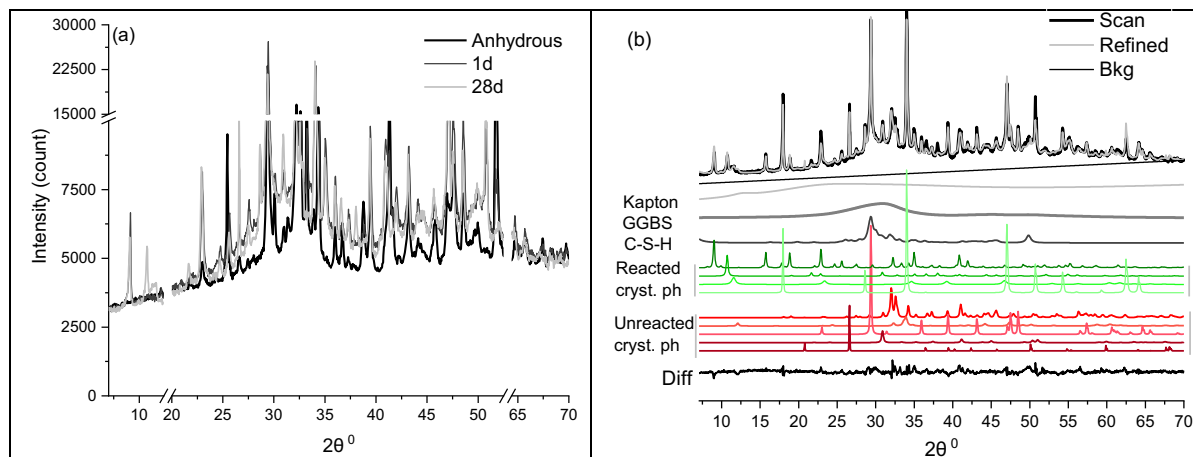


**Fig. 5** **a** Effect of ongoing hydration on the hump associated with GGBS and reflections of crystalline phases in hydrated blended cement, and **b** deconvolution of the crystalline, PONKCS phase for GGBS and C-A-S-H phase in the 28d old freshly ground CS<sub>1</sub>40-L

compared to water. For a given irradiated volume, high free water content (and hence fewer solids) lowers absorption by reducing contributing particles [47, 52]. Furthermore, the water-rich matrix counteracts scattering arising from secondary signals traversing through the matrix, thus improve sharpness of reflections including the hump due to the amorphous phase. Noticeable reduction in the GGBS hump was observed between 1 and 28d, confirming continued hydration. Detailed explanation of the kinetics and phase assemblages are presented elsewhere [19]. A further contributing factor to the diffuse background is the C-A-S-H phase, with a maximum occurring around  $\sim 29$  ( $2\theta^\circ$ ), which simultaneously overlaps with GGBS and calcite, (Fig. 5b).

In addition to being poorly crystalline, the composition of the C-A-S-H phase is also a function of mix composition and hydration degree [53], thus complicating the ability to calibrate with any certainty. Consequently, a 14 Å tobermorite C-S-H model was adopted to represent the C-A-S-H phase, as previously implemented by Bergold et al. [29]. This approximation is justified by the fact that, reflections due to katoite, the main distinguishing feature between the C-S-H and C-A-S-H [54], were not observed in the samples. Consequently, the tobermorite model was implemented without calibrating the ZM constant. The lattice parameters and crystallite size were constrained and refined together with the scale factor, while the unit cell volume and grain size were fixed. Consequently, while supplementing the background as in

[16], the weight fractions of C-A-S-H were not directly measured.

Figure 5b shows the pattern for C-A-S-H and the PONKCS phase for GGBS, contribution from kapton film, together with the hydrates and unreacted crystalline phases. Synthetic mixes of GGBS, corundum and C-S-H with 1.33 and 1.5 Ca/Si ratios were further examined. The amorphous humps of the mixtures were not significantly affected by the different C-S-H Ca/Si ratio despite the anticipated shift towards higher crystallinity with the Ca/Si ratios [40]. A plausible explanation is the high degree of overlap of the C-S-H diffraction pattern with the broader GGBS hump. The calibrated model estimated the GGBS content to about  $\pm 2\%$  in the presence of the C-S-H. Besides the changing C-A-S-H composition, the cement and GGBS grains continue to hydrate over time, modifying the grain characteristics. Consequently, micro-absorption corrections based on grading of anhydrous constituents may be less reliable in the hydrated samples.

### 3.2.2 Amorphization of hydrates

The DTG plots in Fig. 6a and the diffractograms (insert) give an overview of the impact of the various hydration stopping methods on the phase assemblages in blended cements. Decompositions up to 200 °C identify the presence of C-S-H and ettringite. These phases were most sensitive to the hydration stopping method. The loss of free water in the freshly ground

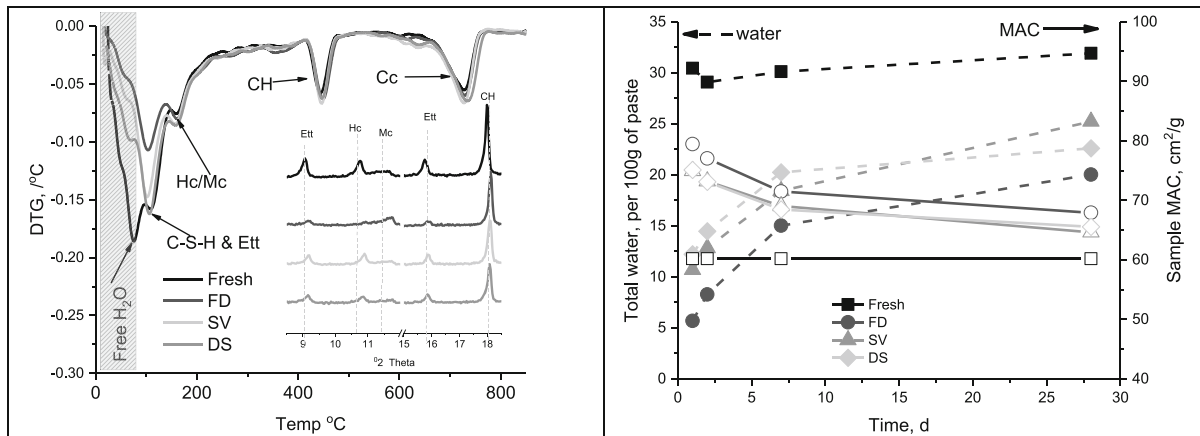


**Fig. 6** Effect of hydration stoppage on **a** thermal decomposition of phases plotted in terms of derivative of thermogravimetric curve and corresponding XRD (insert in a) after 28 d; **b** total water and mean absorption of the sample over the course of

samples, distinct from the chemically bound water, was noticed up to about 80 °C. C-S-H and ettringite decomposition in the solvent exchanged samples were similar, irrespective of whether iso-propanol was removed by vacuum drying or displaced with ether. Meanwhile, freeze-drying was more detrimental than solvent exchange to these phases. The DTG showed significantly weaker C-S-H and ettringite decomposition endotherms, whereas XRD confirmed a much-diminished ettringite reflection after freeze-drying. This effect has been recognized in the literature [12, 38]. The portlandite content appears to be less sensitive to the drying method, consistent with that reported elsewhere [6]. However, the reflections of ettringite and the AFm phases were significantly sharpened in the freshly ground samples (Fig. 6a—insert) due to the micro-absorption contrast as explained above.

Figure 6b shows considerable free-water in the non-hydration stopped, ground sample. It also revealed the excessive removal of free and some bound water upon freeze-drying. The solvent dried samples showed intermediate water contents. In the freshly ground samples, the total water content approximated 33%, as expected at 0.5 w/c, and did not vary significantly with hydration time. The water content measured in the hydration stopped samples meanwhile increased over time, a further indicator of hydration. In all instances, the water contents of the ground, non-hydration stopped samples were greatest.

hydration. Note: Solid symbols with dash lines denote total water content in the sample whilst open symbols with solid lines denote mixture MAC

The water contents of the solvent exchanged samples were 20 to 70% lower at equivalent ages, while the water content of the freeze-dried samples was reduced by 54–84%. In all cases the difference was greatest at early age.

Figure 6b further shows MAC of the cement paste samples calculated from Eq. (7) as a function of hydration stopping method and time. This ranged from ~ 59 to 84 cm<sup>2</sup>/g depending on the total water content in the sample, being highest for freeze-dried pastes and lowest in the freshly ground samples. By having low linear absorption compared to the cement constituents, more water in the sample should decrease the sample mass attenuation co-efficient [47, 52]. However, the combined influence with particle sizes seems to exert greater influence since they together modify the Brindley correction. The situation is more complicated in the hydrating mixes since the PSD of the scanned samples cannot be measured with any certainty, and accounting for sample micro-porosity in the sample absorption calculations is impossible.

The phase contents obtained from Rietveld refinements were corrected for differences in MAC (Fig. 6b) based on Eq. (7). Figure 7a shows ettringite and portlandite contents as a function of hydration stopping method and time. The extent of ettringite amorphization upon freeze-drying was age-dependent with some crystalline ettringite detected in the 28d samples, but not in younger ones. However, ettringite contents from the double solvent exchanged samples

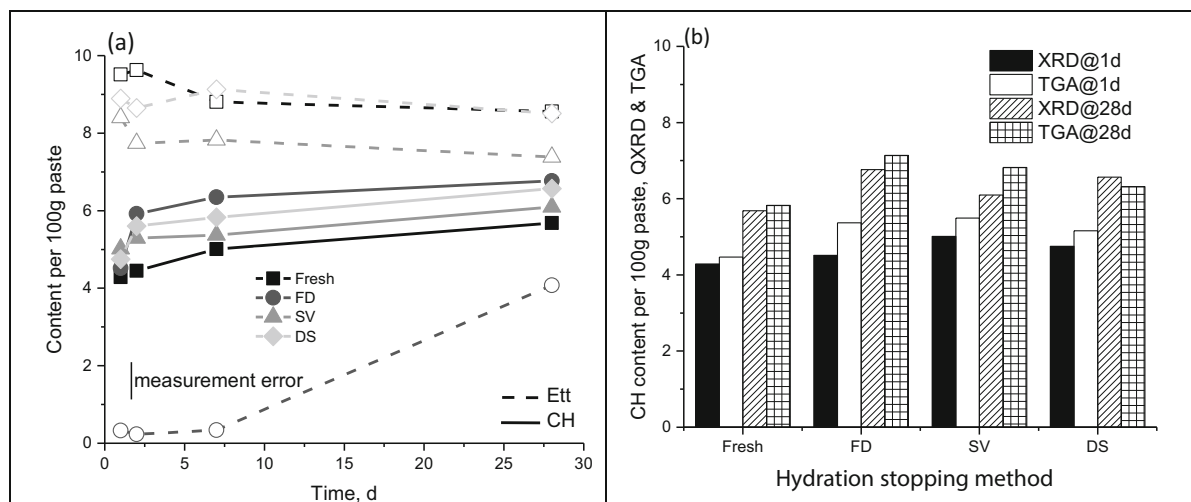


**Fig. 7** Effect of hydration stoppage on **a** the quantitative phase analysis of ettringite (dashed lines) and CH (solid lines) in the course of hydration **b** comparison between the CH content measured by QXRD and TGA

were mostly comparable to the freshly ground samples, suggesting minimal ettringite alteration. Extraction of IPA by vacuum drying was also detrimental to ettringite crystallinity but to a lesser extent than freeze-drying. In the latter, the measured ettringite content at 28d was approximately half that measured in the non-hydration stopped sample, consistent with the previous findings [38]. Modification of phases upon hydration stopping can further confound the background in hydrated cements.

The DTG plots (Fig. 6a) indicated subtle differences in portlandite contents; consistent with previous work [6, 13, 39]. However, Fig. 7a indicates slightly higher CH weight fractions in the hydration-stopped samples, but still within the accuracy of the technique. An assessment of potential modifications in CH contents could be made by comparing results from TGA and XRD. As noticed in Fig. 7b, for a given hydration stopping method and degree of reaction, CH contents from XRD and TG were in close agreement but generally slightly greater when using TGA. This is consistent with nanocrystalline CH being not normally detected by XRD. The double solvent exchange approach showed the closest agreement with freshly ground samples.

Meanwhile, higher contents of monocarboaluminate, were measured in hydration stopped samples compared to freshly ground ones, being highest after freeze-drying. The hemicarboaluminate and hydrotalcite contents were generally below 2% per 100 g of

paste and hence the effect of hydration stopping on these could not be resolved with any certainty.

### 3.2.3 Implementation of the PONKCS Phase on hydrated blended cements

Suitability of the GGBS PONKCS phase (so far calibrated and tested on synthetic mixes and anhydrous blended cements) was assessed in the Rietveld refinement of hydrated blended cement pastes containing 40% GGBS and 10% limestone and 0.5 w/b ratio.

Figure 8a shows the residual anhydrous GGBS contents obtained through the external standard method [35, 36] using the refined scale factors and the corresponding sample specific MAC. The reported weight fractions have been further normalized to the anhydrous binder contents (Eq. 8). Residual GGBS contents reduced due to continued hydration. The rate of reaction was faster at early age, slowing considerably beyond 7d. Detailed explanation of the kinetic controlling mechanisms have been discussed elsewhere [19]. Hydration stopping by solvent exchange yielded results comparable to those from the freshly ground samples. However, freeze-dried samples showed higher anhydrous contents, but the contents were comparable among the different hydration stopping regimes. This suggests lower degree of reaction upon freeze-drying, but this is not the case since identical hydrated sample was subjected to hydration stopping.

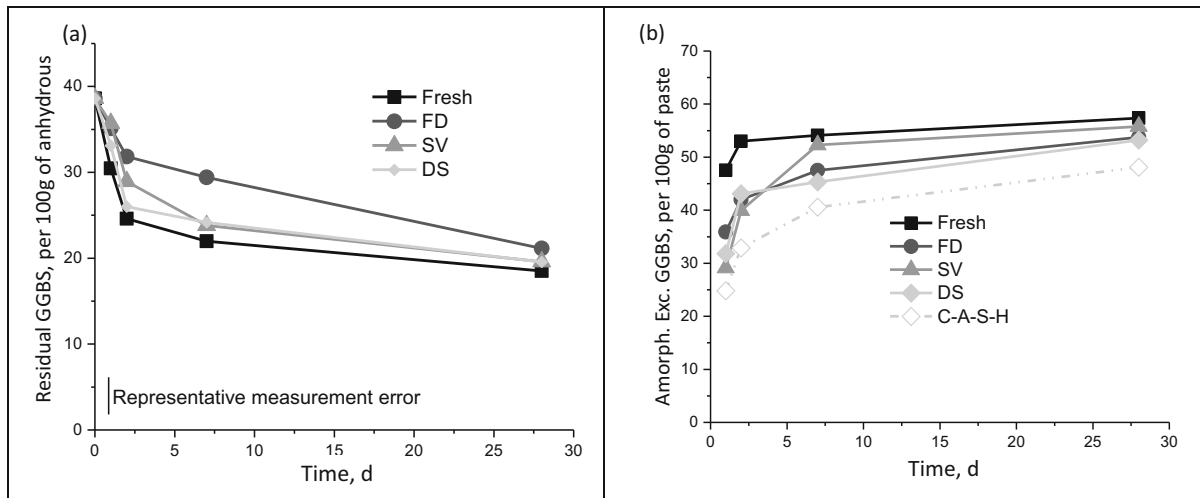


**Fig. 8** Effect of hydration stoppage on: **a** the residual GGBS content and **b** the total amorphous content after Rietveld refinement at different hydration times. Note: C-A-S-H content based on mass balance calculations

To clarify the origin of this higher measured residual GGBS following freeze-drying, the total non-determined contents were obtained by difference [34] and compared with the anticipated C-A-S-H phase content from mass balance calculations [3]. Non-determined contents, including poorly crystalline hydrates e.g. C-A-S-H, dominated all mixes (Fig. 8b). The hydration stopped samples showed lower non-determined contents than the freshly ground samples at early age, but these became comparable at 28 d. However, comparison with the theoretical C-A-S-H content from mass balance (dashed lines in Fig. 8b) suggests the presence of additional amorphous phase(s) in all samples. This may include hydrotalcite, AFm and free water in the case of the freshly ground sample. Higher amorphous content in the fresh sample is also consistent with the higher background noted in Fig. 5.

Next, likelihood of C-A-S-H phase modification by hydration stopping was assessed based on the shift in basal spacing (i.e.  $d_{004}$  and  $d_{002}$ ) at  $\sim 6.9$  and  $29^\circ 2\theta$  respectively [55]. Any changes were slight, with the basal spacing  $d_{004}$  varying from 14.6 and 14.8 Å while  $d_{002}$  was 3.117–3.125 Å without a consistent trend. Consequently, potential structural modifications could not be substantiated. More secondary amorphous content in the freshly ground sample is not surprising considering the excess free water. As hinted earlier, the freeze-dried sample contained higher absorbing phase (solids) per unit volume (see Fig. 6b). Indeed

the effect of micro-absorption on determination of the amorphous content has recently been reported elsewhere [50] suggesting potentially ruinous effect at higher absorption contrasts. While it is difficult, if not impossible, to adequately account for size dependent absorption effects in complex mixtures such as hydrating cement, the adoption of specimen-specific attenuation factors to address compositional contrasts has been shown in this study to improve the precision of the measurements.

### 3.3 Comparison with independent SEM/IA measurement

Impact of hydration stoppage on quantitative phase analysis of the GGBS/PONKCS phase was evaluated against independently obtained SEM/IA of the same hydrated ternary cement. Systematic differences associated with the different regimes (i.e. difference between contents determined from QXRD/PONKCS and SEM/IA) are shown in Fig. 9. The consistently negative difference is due to limitations in SEM/IA resolution meaning that sub-micron particles that are not visible and are assumed to have reacted, leading to underestimation of the residual GGBS contents. Meanwhile, background contributions due to destroyed phase assemblages would increase the amorphous content, causing underestimation of the reacted GGBS. Error of the GGBS content determined by PONKCS compared to SEM/IA ranged between  $\sim$

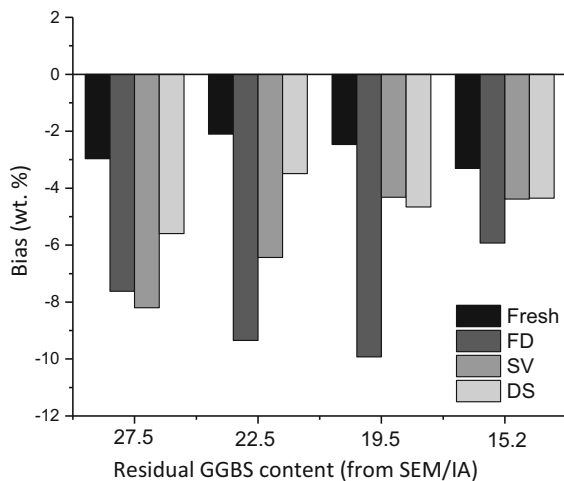


**Fig. 9** Bias of the GGBS contents measured from PONKCS for different hydration stopping regimes compared to that from SEM/IA. Note, bias is calculated as the difference between the GGBS content determined from SEM/IA and that from QXRD/PONKCS analysis after the different treatments

2 to 10%, depending on the sample treatment before XRD (i.e. hydration stopping protocol). A smaller difference was obtained when comparing the PONKCS calculations on the fresh samples to that from SEM/IA. These were within 2–3% of that from SEM/IA. Amongst the hydration-stopped samples however, the smallest bias was measured following the double solvent exchange and the largest upon freeze-drying. It appears that at early age, removal of the solvent via vacuum drying was equally detrimental with respect to quantification of the GGBS content.

#### 4 Concluding remarks

A PONKCS phase for GGBS has been examined in synthetic mixes of varying complexity including blends containing C-S-H. The stability of the phase was further assessed in hydrated ternary blended cement as a function of hydration time and hydration stopping methods.

The results presented here demonstrate the impact on qualitative and quantitative XRD/PONKCS analysis of freeze drying, combined solvent and vacuum drying as well as double exchange hydration stopping protocols compared to freshly ground hydrated cements. The anhydrous or unreacted clinker phases in CEM I were less affected, but quantification of water-rich phase

assemblages e.g., ettringite and AFm were more sensitive to hydration stopping methods. Portlandite contents determined by TGA were consistently greater than XRD, as has previously been observed in the literature, but this was not significantly influenced by the hydration stopping methods investigated. Ettringite and AFm were not preserved entirely by any of the investigated techniques. Freeze-drying was most detrimental, followed by the combined IPA and vacuum drying. Double solvent exchange with IPA and diethyl ether was an improvement as far as water-rich assemblages were concerned and showed closer comparison with the freshly ground non-hydration stopped samples. Residual GGBS contents in the paste samples were successfully measured from the scale factors using the external standard method. Based on the biases of the quantified residual GGBS content from each hydration stopping regime compared to SEM/IA, the use of freshly ground samples without hydration stopping was not prohibitive for implementing the PONKCS phase, which has been modelled and calibrated on anhydrous mixtures. The method of arresting hydration significantly influenced the measured residual GGBS content when the samples were hydration stopped by freeze-drying.

The modelled GGBS phase was distinct from the C-S-H phase despite some overlap between angular ranges where they occur. Comparison between the total water content (Fig. 6b) to the amorphous content excluding GGBS (Fig. 8b) further revealed that the ~ 25% free water per paste (i.e. 33% total) at early age in the freshly ground compared reasonably well with the excess amorphous content from XRD. Once this was accounted for in the MAC calculations, the total non-determined contents were comparable to the double solvent exchange. Considering the complications from hydration stopping, freshly ground samples are recommended for implementing QXRD/PONKCS analysis. However, taking cognisance of techniques and constraints of time-sensitive measurements, double solvent exchange appears to be least detrimental among the considered hydration stopping techniques, achieving < 5% bias compared to SEM/IA.

**Author contributions** Conceptualization: [SAA, MZ, PH, LB], Methodology: [SAA, MZ, PH, LB], Formal analysis and investigation: [SAA, MZ, PH], Writing—original draft preparation: [SAA, PH]; Writing—review and editing: [SAA,



MZ, PH, LB], Funding acquisition: [SAA, MZ, LB], Resources: [SAA, MZ, PH, LB], Supervision: [SAA, MZ, PH, LB].

### Declarations

**Conflict of interest** The authors have no competing interest to declare.

**Open Access** This article is licensed under a Creative Commons Attribution 4.0 International License, which permits use, sharing, adaptation, distribution and reproduction in any medium or format, as long as you give appropriate credit to the original author(s) and the source, provide a link to the Creative Commons licence, and indicate if changes were made. The images or other third party material in this article are included in the article's Creative Commons licence, unless indicated otherwise in a credit line to the material. If material is not included in the article's Creative Commons licence and your intended use is not permitted by statutory regulation or exceeds the permitted use, you will need to obtain permission directly from the copyright holder. To view a copy of this licence, visit <http://creativecommons.org/licenses/by/4.0/>.

### References

- Kocaba V, Gallucci E, Scrivener KL (2012) Methods for determination of degree of reaction of slag in blended cement pastes. *Cem Concr Res* 42:511–525
- Scrivener KL (2004) Backscattered electron imaging of cementitious microstructures: understanding and quantification. *Cem Concr Compos* 26:935–945
- Scrivener KL, Füllmann T, Gallucci E, Walenta G, Bermejo E (2004) Quantitative study of Portland cement hydration by X-ray diffraction/Rietveld analysis and independent methods. *Cem Concr Res* 34:1541–1547
- Scrivener K, Lothenbach B, De Belie N, Gruyaert E, Skibsted J, Snellings R, Vollpracht A (2015) TC 238-SCM: hydration and microstructure of concrete with SCMs. *Mater Struct* 48:835–862
- Durdziński PT, Ben Haha M, Bernal SA, De Belie N, Gruyaert E, Lothenbach B, Menéndez Méndez E, Provis JL, Schöler A, Stabler C, Tan Z, Villagrán Zaccardi Y, Vollpracht A, Winnefeld F, Zajac M, Scrivener KL (2017) Outcomes of the RILEM round robin on degree of reaction of slag and fly ash in blended cements. *Mater Struct* 50:135
- Collier NC, Sharp JH, Milestone NB, Hill J, Godfrey IH (2008) The influence of water removal techniques on the composition and microstructure of hardened cement pastes. *Cem Concr Res* 38:737–744
- Zhang J, Scherer GW (2011) Comparison of methods for arresting hydration of cement. *Cem Concr Res* 41:1024–1036
- Feldman RF, Beaudoin JJ (1991) Pretreatment of hardened hydrated cement pastes for mercury intrusion measurements. *Cem Concr Res* 21:297–308
- Gallé C (2001) Effect of drying on cement-based materials pore structure as identified by mercury intrusion porosimetry: a comparative study between oven-, vacuum-, and freeze-drying. *Cem Concr Res* 31:1467–1477
- Mitchell LD, Margeson JC (2006) The effects of solvents on C-S-H as determined by thermal analysis. *J Therm Anal Calorim* 86:591–594
- Beaudoin JJ, Gu P, Marchand J, Tamtsia B, Myers RE, Liu Z (1998) Solvent replacement studies of hydrated Portland cement systems: the role of calcium hydroxide. *Adv Cem Based Mater* 8:56–65
- Galan I, Beltagui H, García-Maté M, Glasser FP, Imbabi MS (2016) Impact of drying on pore structures in ettringite-rich cements. *Cem Concr Res* 84:85–94
- Snoeck D, Velasco LF, Mignon A, Van Vlierberghe S, Dubruel P, Lodewyckx P, De Belie N (2014) The influence of different drying techniques on the water sorption properties of cement-based materials. *Cem Concr Res* 64:54–62
- Snellings R, Chwast J, Cizer Ö, De Belie N, Dhandapani Y, Durdziński P, Elsen J, Haufe J, Hooton D, Patapy C, Santhanam M, Scrivener K, Snoeck D, Steger L, Tongbo S, Vollpracht A, Winnefeld F, Lothenbach B (2018) Report of TC 238-SCM: hydration stoppage methods for phase assemblage studies of blended cements—results of a round robin test. *Mater Struct* 51:111
- Kakali G, Tsivilis S, Aggeli E, Bati M (2000) Hydration products of C3A, C3S and Portland cement in the presence of CaCO<sub>3</sub>. *Cem Concr Res* 30:1073–1077
- Snellings R, Salze A, Scrivener KL (2014) Use of X-ray diffraction to quantify amorphous supplementary cementitious materials in anhydrous and hydrated blended cements. *Cem Concr Res* 64:89–98
- Machner A, Zajac M, Ben Haha M, Kjellsen KO, Geiker MR, De Weerd K (2018) Chloride-binding capacity of hydrotalcite in cement pastes containing dolomite and metakaolin. *Cement Concr Res* 107:163–181
- Schöler A, Lothenbach B, Winnefeld F, Zajac M (2015) Hydration of quaternary Portland cement blends containing blast-furnace slag, siliceous fly ash and limestone powder. *Cement Concr Compos* 55:374–382
- Adu-Amankwah S, Zajac M, Stabler C, Lothenbach B, Black L (2017) Influence of limestone on the hydration of ternary slag cements. *Cem Concr Res* 100:96–109
- Deschner F, Winnefeld F, Lothenbach B, Seufert S, Schwesig P, Ditttrich S, Goetz-Neunhoeffler F, Neubauer J (2012) Hydration of Portland cement with high replacement by siliceous fly ash. *Cem Concr Res* 42:1389–1400
- De Weerd K, Haha MB, Le Saout G, Kjellsen KO, Justnes H, Lothenbach B (2011) Hydration mechanisms of ternary Portland cements containing limestone powder and fly ash. *Cem Concr Res* 41:279–291
- Durdziński PT, Dunant CF, Haha MB, Scrivener KL (2015) A new quantification method based on SEM-EDS to assess fly ash composition and study the reaction of its individual components in hydrating cement paste. *Cem Concr Res* 73:111–122
- Adu-Amankwah S, Black L, Skocek J, Ben Haha M, Zajac M (2018) Effect of sulfate additions on hydration and performance of ternary slag-limestone composite cements. *Construct Build Mater* 164:451–462
- Ogirigbo OR, Black L (2016) Influence of slag composition and temperature on the hydration and microstructure of slag blended cements. *Constr Build Mater* 126:496–507
- Whittaker M, Zajac M, Ben Haha M, Bullergahn F, Black L (2014) The role of the alumina content of slag, plus the



- presence of additional sulfate on the hydration and microstructure of Portland cement-slag blends. *Cement Concr Res* 66:91–101
26. Rietveld HM (1969) A profile refinement method for nuclear and magnetic structures. *J Appl Cryst* 2:65–71
  27. Bish DL, Howard SA (1988) Quantitative phase analysis using the Rietveld method. *J Appl Cryst* 21:86–91
  28. Scarlett NVY, Madsen IC (2006) Quantification of phases with partial or no known crystal structures. *Powder Diffr* 21:278–284
  29. Bergold ST, Goetz-Neunhoeffler F, Neubauer J (2013) Quantitative analysis of C-S-H in hydrating alite pastes by in-situ XRD. *Cem Concr Res* 53:119–126
  30. Avet F, Li X, Scrivener K (2018) Determination of the amount of reacted metakaolin in calcined clay blends. *Cem Concr Res* 106:40–48
  31. Mejdí M, Wilson W, Saillio M, Chaussadent T, Divet L, Taghit-Hamou A (2020) Quantifying glass powder reaction in blended-cement pastes with the Rietveld-PONKCS method. *Cem Concr Res* 130:105999
  32. Naber C, Stegmeyer S, Jansen D, Goetz-Neunhoeffler F, Neubauer J (2019) The PONKCS method applied for time resolved XRD quantification of supplementary cementitious material reactivity in hydrating mixtures with ordinary Portland cement. *Constr Build Mater* 214:449–457
  33. Hill J, Howard CJ (1987) Quantitative phase analysis from neutron powder diffraction data using the Rietveld method. *J Appl Cryst* 20:467–474
  34. Madsen IC, Scarlett NVY, Kern A (2011) Description and survey of methodologies for the determination of amorphous content via X-ray powder diffraction. *Z Kristallogr* 226(12):944–955. <https://doi.org/10.1524/zkri.2011.1437>
  35. Jansen D, Goetz-Neunhoeffler F, Stabler C, Neubauer J (2011) A remastered external standard method applied to the quantification of early OPC hydration. *Cem Concr Res* 41:602–608
  36. O'Connor BH, Raven MD (1988) Application of the rietveld refinement procedure in assaying powdered mixtures. *Powder Diffr* 3:2–6
  37. Creagh DC, Hubbell JH (2006) X-ray absorption (or attenuation) coefficients. *Int Tables Crystallogr C* 220–229
  38. Zhang L, Glasser FP (2000) Critical examination of drying damage to cement pastes. *Adv Cem Res* 12:79–88
  39. Thomas MDA (1989) The suitability of solvent exchange techniques for studying the pore structure of hardened cement paste. *Adv Cem Res* 2:29–34
  40. Tajuelo Rodriguez E, Garbev K, Merz D, Black L, Richardson IG (2017) Thermal stability of C-S-H phases and applicability of Richardson and Groves' and Richardson C-(A)-S-H(I) models to synthetic C-S-H. *Cement Concr Res* 93:45–56
  41. Le Saoût G, Kocaba V, Scrivener K (2011) Application of the Rietveld method to the analysis of anhydrous cement. *Cem Concr Res* 41:133–148
  42. Cheary RW, Coelho AA, Cline JP (2004) Fundamental parameters line profile fitting in laboratory diffractometers. *J Res Natl Inst Stand Technol* 109:1–25
  43. Maslen EN, Streltsov VA, Streltsova NR (1993) X-ray study of the electron density in calcite,  $\text{CaCO}_3$ . *Acta Cryst B* 49:636–641
  44. Page YL, Donnay G (1976) Refinement of the crystal structure of low-quartz. *Acta Cryst B* 32:2456–2459
  45. Pawley GS (1981) Unit-cell refinement from powder diffraction scans. *J Appl Cryst* 14:357–361
  46. Gutteridge WA (1979) On the dissolution of the interstitial phases in Portland cement. *Cem Concr Res* 9:319–324
  47. Alexander L, Klug HP (1948) Basic aspects of X-ray absorption in quantitative diffraction analysis of powder mixtures. *Anal Chem* 20:886–889
  48. Durdziński PT, Ben Haha M, Zajac M, Scrivener KL (2017) Phase assemblage of composite cements. *Cement Concr Res* 99:172–182
  49. Snellings R, Bazzoni A, Scrivener K (2014) The existence of amorphous phase in Portland cements: physical factors affecting Rietveld quantitative phase analysis. *Cem Concr Res* 59:139–146
  50. Scarlett N, Madsen I (2018) Effect of microabsorption on the determination of amorphous content via powder X-ray diffraction. *Powder Diffr* 33:26–37
  51. Brindley GW (1945) The effect of grain or particle size on X-ray reflections from mixed powders and alloys, considered in relation to the quantitative determination of crystalline substances by X-ray methods. *Philos Mag* 36:347–369
  52. Manjunath BR, Venkataraman A, Stephen T (1973) The effect of moisture present in polymers on their X-ray diffraction patterns. *J Appl Polym Sci* 17:1091–1099
  53. Richardson IG, Groves GW (1997) The structure of the calcium silicate hydrate phases present in hardened pastes of white Portland cement/blast-furnace slag blends. *J Mater Sci* 32:4793–4802
  54. L'Hôpital E, Lothenbach B, Le Saout G, Kulik D, Scrivener K (2015) Incorporation of aluminium in calcium-silicate-hydrates. *Cem Concr Res* 75:91–103
  55. L'Hôpital E, Lothenbach B, Scrivener K, Kulik DA (2016) Alkali uptake in calcium alumina silicate hydrate (C-A-S-H). *Cem Concr Res* 85:122–136

**Publisher's Note** Springer Nature remains neutral with regard to jurisdictional claims in published maps and institutional affiliations.

